Structure Prediction of Li–Sn and Li–Sb Intermetallics for Lithium-ion Batteries Anodes.

Martin Mayo[†] and Andrew J. Morris[*,†,‡]

Theory of Condensed Matter Group, Cavendish Laboratory, University of Cambridge, J. J. Thomson Avenue, Cambridge CB3 0HE, United Kingdom, and Department of Physics, University of Warwick, Coventry, CV4 7AL, United Kingdom

E-mail: ajm255@cam.ac.uk

Abstract

A variety of new stable and metastable Li–Sn and Li–Sb intermetallics are presented using the *ab initio* random structure searching (AIRSS) and species swapping methods. There include $LiSn_2$–$P4/mmm$, Li_2Sn_3–$P\bar{1}$, Li_7Sn_9–$P4_2/n$, Li_3Sn_2–$P2_1/m$, Li_5Sn_3–$Im\bar{3}m$, Li_2Sn–$Cmcm$, Li_8Sn_3–$R\bar{3}m$, Li_3Sn–$P3_2$, Li_7Sn_2–$P\bar{1}$, Li_4Sn–$P2_1$, Li_5Sn–$P6/mmm$, Li_7Sn–$Fmmm$, LiSb–$P4/mmm$, Li_8Sb_5–$Fd\bar{3}m$, Li_8Sb_3–$P2/c$, Li_4Sb–C2/m, Li_9Sb_2–$P\bar{3}m_1$, Li_5Sb–$P6/mmm$, Li_6Sb–$R\bar{3}m$, Li_8Sb–Pc and Li_9Sb–$Cmcm$. The Li–Sn theoretical voltage curve was calculated to high–accuracy mainly from experimentally known structures and shows excellent agreement with experimental electrochemical cycling measurements previously reported. Li_2Sn was found on the convex hull to within density–functional theory accuracy and its mechanical stability was investigated by calculating the density of states of the phonon spectrum. The new structures obtained by AIRSS show a consistent structural evolution of Li–Sn phases as Li concentration is increased. First principles NMR calculations on the hexagonal– and cubic–Li_3Sb

[*]To whom correspondence should be addressed
[†]University of Cambridge
[‡]University of Warwick

phases are performed. Our NMR results are compared to findings of Johnston *et al.*, *Chemistry of Materials* (2016) *28*, 4032 and proposed as a diagnostic tool to interpret experimental data.

Introduction

Li–Sn –Sb intermetallics have received renewed attention in recent years, particularly in the field of Li–ion batteries (LIBs), where Sn and Sb have been suggested as potential Li–alloy candidates to replace the currently used graphite intercalation anodes.[1] The binary Li–Sn phase diagram[2] shows the existence of Li_2Sn_5, LiSn, Li_7Sn_3, Li_5Sn_2, $Li_{13}Sn_5$, Li_7Sn_2, and $Li_{22}Sn_5$. However, a more accurate description of $Li_{22}Sn_5$ was suggested to be $Li_{17}Sn_4$.[3] A voltage curve of Li–Sn using a coulometric titration technique was presented by Wang *et al.*[4] at 25 ^{o}C and 400 ^{o}C. At 400 ^{o}C the Li_5Sn_2 phase found at 25 ^{o}C was no longer present and a Li_2Sn_5 phase arose. Courtney *et al.*[5] performed an *ab initio* calculation of the voltage curve considering the known experimental Li–Sn structures. They showed good agreement with experiment up to $x = 2.5$ in Li_xSn. However, the calculated voltage increased at $x = 2.5$ due to a metastable Li_5Sn_2 phase included in the calculation and was followed by a sharp drop at $x = 2.6$, which makes the match between curves around this point questionable. It was suggested that for $x > 2.5$ the structure adopted a body–centered cubic–like lattice with Li and Sn atoms similarly as seen in $Li_{22}Sn_5$, but with short range order characteristics. A more recent comparison between experimental and calculated voltage curves using known phases was reported by Tran *et al.*[6] by using formation energies directly from the Materials Project.[7] A fairly good agreement was shown up to $x = 2.5$ and a deviation from the experiment was seen at larger Li concentration values. We note that default k–point setting used in the 1.x versions of the Materials Project might have been inadequate to properly sample the Brillouin zone of metallics systems, resulting in inaccurate formation energies.

Unlike the Li–Sn case where many phases are present, only two are reported in the Li–Sb phase diagram:[8] Li_2Sb and Li_3Sb. Two polymorphs of Li_3Sb have been reported: an ambient pressure hexagonal $P6_3/mmc$ phase and a high–pressure cubic $Fm\bar{3}m$ one. Upon lithiation of Sb,

two plateaus are observed which correspond to Li_2Sb and Li_3Sb.[9] Interestingly, both the cubic and hexagonal phases have been shown to form electrochemically.[9,10] During delithiation, Li_2Sb is generally no longer observed and Li_3Sb is converted directly to Sb, leading to hysteresis in the voltage curve.[11] The origin of the hysteresis has been discussed recently by Chang *et al.*[12]

Compound Sn–Sb phases have also been considered as potential anodes for LIBs in several works (see references in Ref. 1) and have shown improved electrochemical performance. The plateaus observed in the voltage curve have been attributed mainly to multi–phase reactions usually involving Li_xSb / Li_xSn phases (see for example Ref. 13). TiSnSb has also received attention in the context of anode materials for LIBs, where a reversible capacity of 540 mA h g^{-1} and 4070 mA h cm^{-3} at 2C rate and good cyclability were reported.[14,15] The proposed lithiation mechanism in TiSnSb involves the formation of different Li–Sn and Li–Sb phases, some of them thought to be metastable with an as–yet unknown crystalline structure.[14,15]

In this paper, we present a structure prediction study of Li–Sn and Li–Sb intermetallics by combining the *ab initio* random structure searching method (AIRSS) with high–throughput screening from the International Crystal Structure Database (ICSD). We describe new stable and metastable phases predicted by our method including new Li_8Sn_3–$R\bar{3}m$ and Li_7Sn_2–$P\bar{1}$ phases which lie on the convex hull construction. We discuss the implication of these structures to the theoretically obtained voltage curve and compare to previous experimental studies. A study of the mechanical stability of a new Li_2Sn phase obtained by AIRSS is presented. We conclude with NMR calculations of the hexagonal– and cubic–Li_3Sb compounds which are compared to experimental findings observed in Ref. 15.

Methods

The structure prediction was performed by combining the atom–swapping method and AIRSS.[16] To gain initial understanding of the system, all combinations of {Li,Na,K}–{Si,Ge,Sn,Pb} and {Li,Na,K}–{P,As,Sb,Bi} crystal structures at different stoichiometries were obtained from the

ICSD. For each structure, the anions and cations were swapped to Li and Sn from the set of {Li,Na,K} and {Si,Ge,Sn,Pb}, respectively, and to Sb from {P,As,Sb,Bi}. The resulting structures were then relaxed using Hellman–Feynman forces calculated from DFT. Subsequently, an AIRSS search was performed to fill gaps in the phase diagram which resulted in the discovery of new phases. The AIRSS method enables wide coverage of the potential energy surface of the system by relaxing randomly generated structures to a local minimum. Based on general physical principles and system–specific constraints, the search can be biased in a variety of sensible ways.[17] This AIRSS + species swapping method has been successfully used for Li–Si,[18] Li–Ge,[18,19] Li–S,[20] Li–P[21] and Li–MoS_2[22] systems. Furthermore, a study on point defects in silicon has been presented[23] using the AIRSS method.

Approximately 9000 Li–Sn structures and 5000 Li–Sb structures were generated by AIRSS. The calculations were undertaken using the CASTEP DFT plane–wave code[24] using the gradient corrected Perdew–Burke–Ernzerhof (PBE) exchange-corelation functional.[25] The core electrons were described using Vanderbilt "ultrasoft" pseudopotentials. Initially, the Brillouin zone (BZ) was sampled using a Monkhorst-Pack grid[26] with a BZ integration grid spacing finer than $2\pi \times 0.05$ Å^{-1} and the plane wave basis set was truncated at an energy cutoff value of 500 eV for both systems. The low energy structures obtained in the initial search were then refined with higher accuracy using a k–point spacing finer than $2\pi \times 0.03$Å^{-1} and an energy cut–off of 800 eV along with more accurate pseudopotentials[1]. This level of accuracy was used to calculate all properties throughout this study, unless stated otherwise.

The system's thermodynamical phase stability was assessed by comparing the free energy of different phases. From the available DFT total energy, $E\{\mathrm{A}_a\mathrm{B}_b\}$, of a given binary phase of elements A and B with stoichiometry $\mathrm{A}_a\mathrm{B}_b$, it is possible to define a formation energy per atom,

$$E_f/\mathrm{atom} = \frac{E\{\mathrm{A}_a\mathrm{B}_b\} - aE\{\mathrm{A}\} - bE\{\mathrm{B}\}}{a+b}. \quad (1)$$

[1]Pseudopotentials generated by the CASTEP on–the–fly generator:
Li 1|1.2|10|15|20|10U:20(qc=6)
Sn 3|2.2|10|15|20|50:51:42
Sb 3|2.2|10|15|20|50:51:42(compat7)

The formation energies of each structure were plotted as a function of the A element concentration, $u = \frac{a}{a+b}$, starting at $u = 0$ and ending at $u = 1$. A convex hull was constructed between the chemical potentials at $(u, E_f/\text{atom}) = (0,0)$ and $(1,0)$ drawing a tie–line that joins the lowest energy structures, provided that it forms a convex function. This construction gives access to the 0 K stable structure since the second law of thermodynamics demands that the (free) energy per atom is a convex function of the relative concentrations of the atoms (see Figure 1).

Average voltages for the structures lying on the hull were calculated from the available DFT total energies. For two given phases on the hull, $A_{x_1}B$ and $A_{x_2}B$ with $x_2 > x_1$, the following two phase reaction was assumed,

$$A_{x_1}B + (x_2 - x_1)A \rightarrow A_{x_2}B. \tag{2}$$

The voltage, V, for a monovalent carrier is given by,

$$\begin{aligned} V &= -\frac{\Delta G}{x_2 - x_1} \approx -\frac{\Delta E}{x_2 - x_1} \\ &= -\frac{E(A_{x_2}B) - E(A_{x_1}B)}{x_2 - x_1} + E(A), \end{aligned} \tag{3}$$

where it is assumed that the Gibbs energy can be approximated by the internal energy, as the pV and thermal energy contributions are small.[27]

NMR chemical shielding was calculated using the Gauge Including Projector Augmented Wave (GIPAW) algorithm[28] implemented in CASTEP. The ^{7}Li shifts were referenced using a secondary reference, Li_2CO_3, at +1.1 ppm versus the 1.0 M LiCl (aq) primary reference at 0.0 ppm.

Phonon dispersion curves were calculated using Density–functional perturbation theory in CASTEP[29] using norm-conserving pseudopotentials[2], the BZ was sampled using a Monkhorst-Pack grid[26] with a k–point spacing finer than $2\pi \times 0.03$ Å^{-1} and the plane wave basis set was truncated at an energy cut–off of 1200 eV. The structures were fully relaxed at this level of accuracy.

[2]Pseudopotentials generated by the CASTEP on–the–fly generator:
Li 1|1.2|18|21|24|10N:20N(qc=8)
Sn 3|2.4|12|14|16|50N:51N:42N(qc=8)

Results

Lithium Stanides

In Figure 1 we present a plot of formation energy as a function of Li concentration for structures obtained by the combined AIRSS and species swapping method. For clarity, only the lowest–energy structures within 20 meV/atom from the convex hull were included. The convex hull construc-

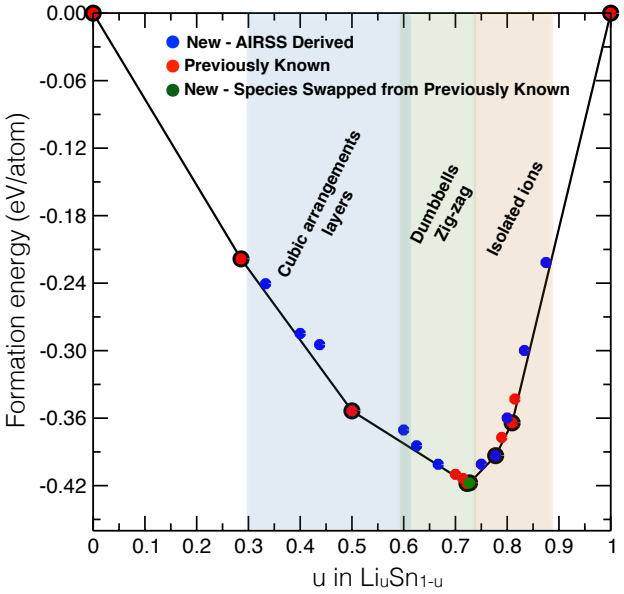

Figure 1: Formation energy per atom versus the fractional Li concentration in the Li–Sn compound. The convex hull (tie–line) is constructed by joining the stable structures obtained by the searches. Only the lowest energy structure for each composition within 20 meV/atom from the convex hull is shown. Blue dots are for structures obtained by AIRSS, red dots for previously known structures and green dots for new structures obtained by swapping species from previously know phases. The phase diagram has been divided into regions illustrating the trends in the ionic arrangements obtained by the structure prediction study.

tion reveals a variety of new phases which were not experimentally reported. A description of the structures is given in Table 1.

Low Li–content structures – $x < 1$ in Li_xSn

AIRSS finds three new structures with a small positive energy above the tie–line, well within DFT accuracy, in the range Li_xSn $x \leq 1$: $LiSn_2$, Li_2Sn_3 and Li_7Sn_9.

Table 1: Description of the experimental and predicted Li_xSn phases found within 20 meV/atom from the convex hull. We indicate with a star ($\star$) the most energetically favourable phases which are found on the convex hull.The CIF files of the structures obtained by AIRSS and the swapping method can be found in the Supporting Information.

Stoichiometry	x in Li_xSn	Distance from the hull [meV/atom]	Space group	Structure origin
Sn$\star$	0.0	0	$I4_1/amd$	
$Li_2Sn_5\star$	0.4	0	$P4/mbm$	Known phase[30]
$LiSn_2$	0.5	8	$P4/mmm$	AIRSS structure
Li_2Sn_3	0.6	6	$P\bar{1}$	AIRSS structure
Li_7Sn_9	0.8	19	$P4_2/n$	AIRSS structure
LiSn $\star$	1.0	0	$P2/m$	Known phase[31]
Li_3Sn_2	1.5	12	$P2_1/m$	AIRSS structure
Li_5Sn_3	1.7	5	$Im\bar{3}m$	AIRSS structure
Li_2Sn	2.0	1	$Cmcm$	AIRSS structure
Li_7Sn_3	2.3	2	$P2_1/m$	Known phase[32]
Li_5Sn_2	2.5	2	$R\bar{3}m$	Known phase[33]
$Li_{13}Sn_5\star$	2.6	0	$P\bar{3}m_1$	Known phase[34]
Li_8Sn_3 $\star$	2.7	0	$R\bar{3}m$	Swap from Li_8Pb_3[35]
Li_3Sn	3.0	6	$P3_2$	AIRSS structure
Li_7Sn_2 $\star$	3.5	0	$P\bar{1}$	AIRSS structure
		6	$Cmmm$	Known phase[36]
$Li_{15}Sn_4$	3.8	6	$I\bar{4}3d$	Known phase[37]
Li_4Sn	4.0	13	$P2_1$	AIRSS structure
$Li_{17}Sn_4\star$	4.25	0	$F\bar{4}3m$	Known phase[3]
$Li_{22}Sn_5$	4.4	11	$F\bar{4}3m$	Known phase[38]
Li_5Sn	5.0	19	$Pmma$	AIRSS structure
Li_7Sn	7.0	18	$C2$	AIRSS structure
Li $\star$		0	$Im\bar{3}m$	

$LiSn_2$–$P4/mmm$ appears 8 meV/atom from the tie–line. The structure has a double–layer of Sn with intercalated Li as can be seen in Figure 2 a.

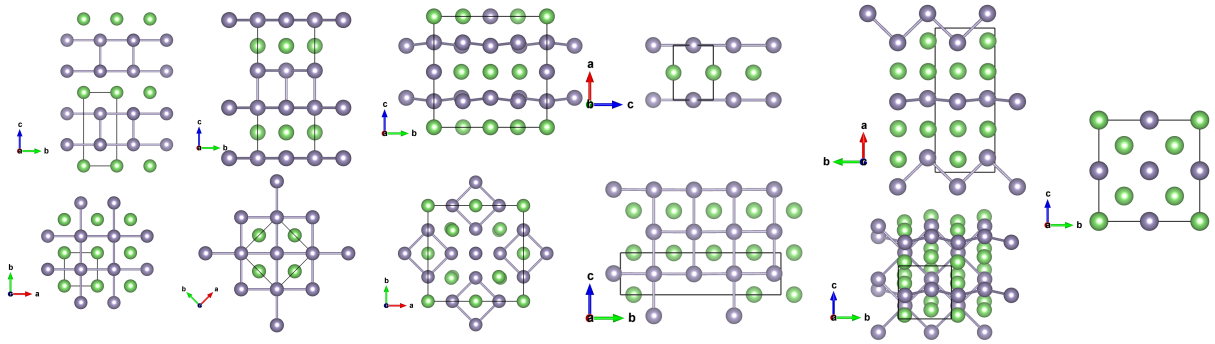

a) $LiSn_2$–$P4/mmm$ b) Li_2Sn_3–$P\bar{1}$ c) Li_7Sn_9–$P4_2/n$ d) Li_1Sn_1–$Pmm2$ e) Li_3Sn_2–$P2_1/m$ f) Li_5Sn_3–$Im\bar{3}m$

Figure 2: Structures found by AIRSS within $0 < x \leq 1.7$ in Li_xSn which exhibit layer–like Sn structures. a) $LiSn_2$–$P4/mmm$ is found 8 meV/atom from the convex hull. It features double layers of Sn ions with cubic angles and intercalated Li in-between. b) The Li_2Sn_3–$P4/mmm$ phase is predicted by AIRSS 6 meV/atom above the convex hull. The structure shows alternate double– and single–layers of four–membered rings of Sn atoms arranged in a cubic geometry. c) Li_7Sn_9–$P4_2/n$ showing distorted two–dimensional sheets of Sn atoms linked by an Sn atom between the layers at the edge of the primitive cells. Flat sheets of Li are intercalated between the Sn layers. d) Li_1Sn_1–$Pmm2$ structure discovered by AIRSS showing layers of Sn atoms arranged in a cubic fashion with intercalated sheets of Li in-between. e) Li_3Sn_2–$P2_1/m$ structure obtained by AIRSS formed of intercalated zigzag-like Sn ions and almost flat Sn sheets. f) Li_5Sn_3–$P\bar{4}_3m$ is an AIRSS structure found 1.7 meV/atom from the convex hull. Sn ions form a three dimensional cubic arrangement and a Li bcc–like sub–lattice. Green and purple spheres denote Li and Sn atoms, respectively, with the purple lines indicating Sn–Sn bonds.

Li_2Sn_3–$P\bar{1}$ is 6 meV/atom above the convex hull tie–line. The structure shows a similar ionic arrangement as the one observed in $LiSn_2$–$P4/mmm$: double and single layers of four–membered rings of Sn atoms arranged in a cubic symmetry alternating (ABAB...) as seen in Fig 2 b.

Li_7Sn_9–$P4_2/n$ is found 19 meV/atom from the tie–line. The structure is composed of distorted two–dimensional sheets of Sn atoms linked by a Sn atom at the edge of the primitive cells between the layers. Flat sheets of Li are intercalated between the Sn layers. An illustration of the structure can be seen in Figure 2 c.

Structures between $1 \leq x \leq 4.4$ in Li_xSn

Two stable polymorphs are known to exist between $1 \leq x \leq 4.4$ in Li_xSn, α–Li_1Sn_1–P2/m[31] and β–Li_1Sn_1–I41/amd.[39] AIRSS has found a new Li_1Sn_1–*Pmm*2 structure comparable energetically at 0 K with the reported ones, as listed in Table 2. The new Li_1Sn_1 structure features layers of Sn

Table 2: Li_1Sn_1 structures' formation energies relative to the experimentally reported α–Li_1Sn_1–$P2/m$. AIRSS has found a new Li_1Sn_1–*Pmm*2 structure comparable energetically at 0 K with the experimentally known α– and β–Li_1Sn_1 phases. The new Li_1Sn_1 structure features layers of Sn atoms arranged in a cubic fashion with intercalated sheets of Li in-between as seen in Figure 2 d.

Relative formation energy [meV/f.u.]	Symmetry	Volume [Å^3/f.u.]	Description
0	$P2/m$	41.83	Known phase[31]
14	$Pmm2$	41.87	AIRSS structure
17	$I4_1/amd$	42.84	Known phase[39]

atoms arranged in a cubic fashion with intercalated sheets of Li in-between (See Figure 2 d). The indistinguishable energy differences between the *Pmm*2 and the reported α and β phases, suggest that Li_1Sn_1–*Pmm*2 is thermodynamically stable at 0 K.

In addition to Li_1Sn_1, this region shows a variety of new structures very close to the convex hull (see Table 1 for details). Li_3Sn_2–$P2_1/m$, Li_5Sn_3–$P\bar{4}3m$, Li_2Sn–*Cmcm*, Li_3Sn–$P3_2$ and Li_4Sn–$P2_1$ were found by AIRSS. Li_3Sn_2–$P2_1/m$ is formed of intercalated zigzag–like Sn ions and almost flat Sn sheets. (See Figure 2 e.)

The tendency of the Li–Sn metastable phases to form cubic–like arrangements is again observed in Li_5Sn_3–$Im\bar{3}m$. The Sn ions are found to be arranged in a three–dimensional cubic arrangement and Li forms a bcc–like sub–lattice as seen in Fig. 2 f.

The Li_2Sn–*Cmcm* phase is found 1 meV/atom above the hull. The structure is formed by in–plane zigzag–like Sn ions as seen in Fig. 3 a and b. Since Li_2Sn–*Cmcm* has not been found before we studied its dynamical stability by calculating the full density of states (phonon spectrum) as presented in Figure 3 c.

The convex hull construction predicts a Li_8Sn_3–$R\bar{3}m$ structure to be stable at 0 K. The struc-

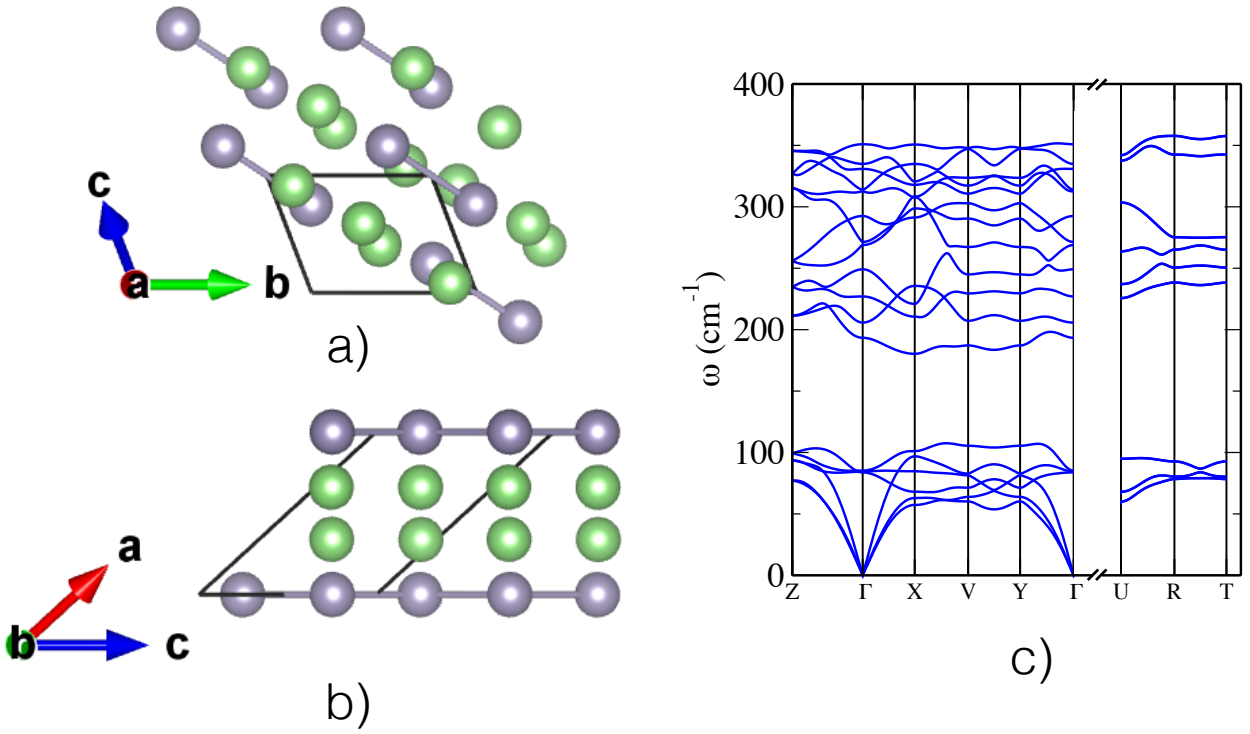

Figure 3: Li_2Sn–*Cmcm* is found 1 meV/atom from the convex hull (effectively indistinguishable from the hull within DFT accuracy). The structure is formed by in-plane zigzag-like Sn ions viewed from a) a direction and b) b direction. c) The mechanical stability of the structure has been investigated by means of its phonon spectrum, where no soft or negative modes were found. Green and purple spheres denote Li and Sn atoms, respectively, with the purple lines indicating Sn–Sn bonds.

ture was obtained by swapping the Pb ions in Li_8Pb_3 [35] to Sn. The structure presents Sn dumbbells combined with isolated Sn atoms as shown in Figure 4. AIRSS predicts a Li_7Sn_2–$P\bar{1}$ phase 6

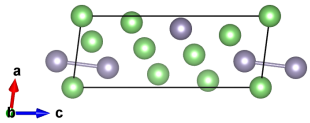

Figure 4: Li_8Sn_3–$C2/m$ is a structure obtained by swapping the Pb ions in Li_8Pb_3 [35] to Sn. The structure is predicted to be stable according to the convex hull construction at 0 K and features Sn dumbbells combined with isolated Sn atoms. Green and purple spheres denote Li and Sn atoms, respectively, with the purple lines indicating Sn–Sn bonds.

meV/atom lower in formation energy than the experimentally reported *Cmmm* phase. This difference remains unchanged after using a finer k–point sampling, increased energy cut–off and larger fast Fourier transform grids, suggesting that the energy difference is fully converged at the PBE level of theory. The Li_7Sn_2–$P\bar{1}$ structure contains isolated Sn ions and an illustration of the structures is presented in Figure 5. The higher Li content structures in this region, Li_3Sn and Li_4Sn,

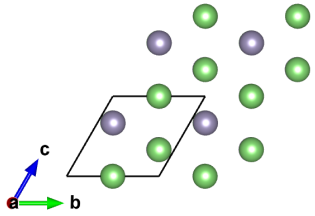

Figure 5: The Li_7Sn_2–$P\bar{1}$ structure is predicted to be stable according to he convex hull construction at 0 K. The structures shows isolated Sn atoms embedded in a seat of Li. Green and purple spheres denote Li and Sn atoms, respectively.

comprise isolated Sn atoms.

High Li–content structures

The predicted Li–Sn phase diagram reveals metastable structures predicted by AIRSS which are found closer than 20 meV to the convex hull at stoichiometries of $x = 5$ and 7 in Li_xSn. All the structures contain Sn atoms dispersed in a sea of Li atoms.

Implications for theoretical voltage curve

In Figure 6 we present for comparison the voltage curve calculated from the stable structures obtained here and the reported voltage curves in Refs. 4 and 5.

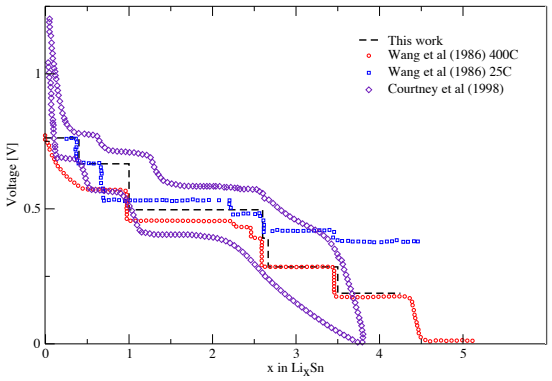

Figure 6: Li–Sn average voltages relative to Li metal calculated for the structures found on the convex hull (Fig. 1). The theoretical voltage curve follows the coulometric titration experiment reported in Ref. 4 at 400°C for $x > 1$. The discrepancy between the calculated and experimental (coulometric titration) voltage curves in $2 < x < 2.6$ arises from the fact that Li_7Sn_3 and Li_5Sn_2 were not included in the voltage curve calculation, since only structures on the hull were used. The 400°C experimental curve shows a drop at $x = 0.66$ which is not described by the calculated voltage curve. AIRSS predicts a metastable Li_2Sn_3–$P\bar{1}$ structure which could be responsible for the observed phase transition.

Lithium Antimonides

A plot of formation energy per atom as a function of Li concentration for the Li–Sb system is presented in Figure 7. We have included the lowest–energy structures within 30 meV/atom from the convex hull which are described in Table 3. No structures from species swapping were found in this range. In addition to the experimentally known Li_2Sb and Li_3Sb phases, AIRSS predicts three metastable structures within 30 meV/atom from the convex hull in the range of $x < 3$ in Li_3Sb: Li_1Sb_1–$P4/mmm$, Li_8Sb_5–$Fd\bar{3}m$ and Li_8Sb_3–P_2/c. Li_1Sb_1–$P4/mmm$ is formed of sheets of cubic–arranged Sb (see Fig. 8), similar to Li_1Sn_1–$P4/mmm$ listed in Table 2. Li_8Sb_5–$Fd\bar{3}m$

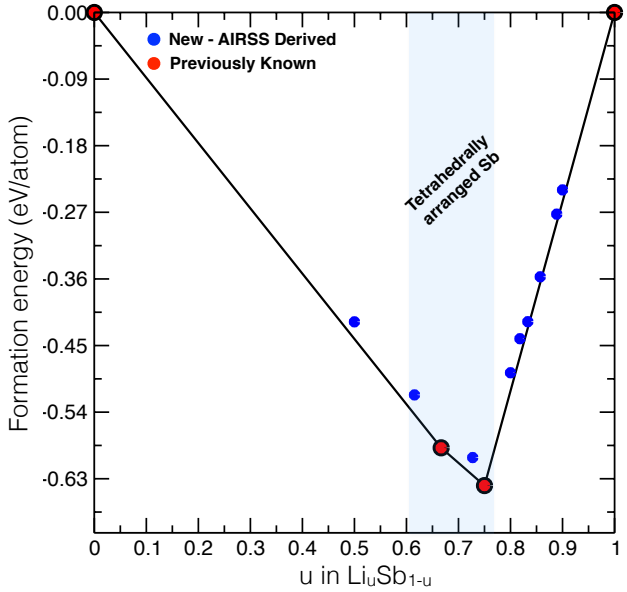

Figure 7: Formation energy per atom versus the fractional Li concentration in the Li–Sb compound. The convex hull (tie–line) is constructed by joining the stable structures obtained by the searches. Only the lowest energy structure for each composition within 0.03 eV from the convex hull are shown.

Table 3: Description of the experimental and predicted Li_xSb phases found within 0.03 eV/fu from the convex hull. We indicate with a star ($\star$) the most energetically favourable phases which are found on the convex hull. The CIF files of the structures obtained by AIRSS and the swapping method can be found in the Supporting Information.

Stoichiometry	x in Li_xSb	Distance from the hull [meV/atom]	Space group	Structure origin
Sb	0	0	$R\bar{3}m$	
LiSb	1	23	$P4/mmm$	AIRSS
Li_8Sb_5	1.6	26	$Fd\bar{3}m$	AIRSS
$Li_2Sb\star$	2	0	$P\bar{6}2c$	Known phase[40]
Li_8Sb_3	2.6	24	$P2/c$	AIRSS
$Li_3Sb\star$	3	0	$Fm\bar{3}m$	Known phase[41]
Li_4Sb	4	25	$C2/m$	AIRSS
Li_9Sb_2	4.5	24	$P\bar{3}m_1$	AIRSS
Li_5Sb	5	8	$P6/mmm$	AIRSS
Li_6Sb	6	8	$R\bar{3}m$	AIRSS
Li_8Sb	8	12	Pc	AIRSS
Li_9Sb	9	16	$Cmcm$	AIRSS
Li		0	$Im\bar{3}m$	

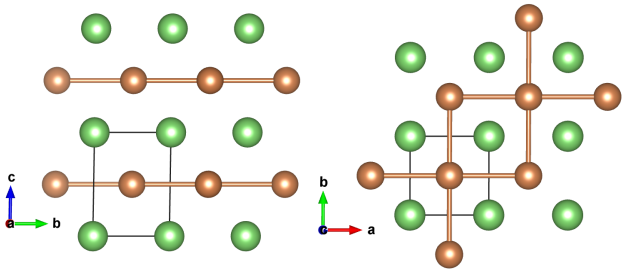

Figure 8: Li_1Sb_1–P4/mmm structure discovered by AIRSS showing layers of Sb atoms arranged in a cubic fashion with intercalated sheets of Li in-between. Green and brown spheres denote Li and Sb atoms, respectively, with the brown lines indicating Sb–Sb bonds.

and Li_8Sb_3–$P2/c$ feature Li ions with four tetrahedrally arranged Sb neighbours. An illustration of the structures is presented in Figure 9.

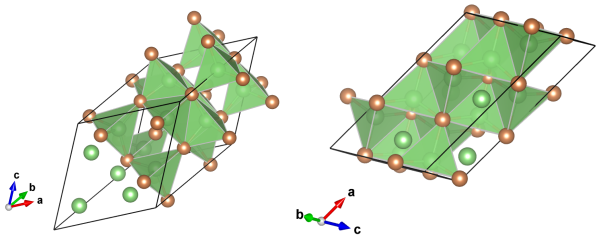

Figure 9: Li_8Sb_5–Fd-3m and Li_8Sb_3–P2/c found by AIRSS within 0.03 meV/atom from the convex hull. The structures show Li ions tetrahedrally bonded to Sb. Green and brown spheres denote Li and Sb atoms, respectively.

The Li–Sb system presents a wide variety of metastable structures very close to the hull tie line at high–Li concentration, including $x = 4, 4.5, 5, 6, 8, 9$. Remarkably, AIRSS managed to find structures very close to the convex hull at almost all attempted stoichiometries in this regime, suggesting that insertion of antimony into amorphous lithium is favourable entropically.

Discussion

The Li–Sn phase diagram presents a large variety of structures within 20 meV/atom from the convex hull. Having access to metastable structures has been shown to be extremely insightful when studying electrochemical processes, since these might occur far from equilibrium. AIRSS was able to reveal a pattern in the metastable structures for increasing Li content. By visual inspection, all

the experimentally known and new derived structures obey the same structural trend which can be interpreted in terms of: cubically arranged layers $\rightarrow$ zig-zag chains + dumbbells $\rightarrow$ isolated atoms. Structural trends in lithium intermetalics have been observed in a variety of studies performed by us, such as the Li–Ge,[19] Li–S[20] and Li–P[21] systems, where the understanding of general structural changes upon lithiation played a critical role in the interpretation of high–resolution experiments. For example, this has been demonstrated in the interpretation of the continuous shift of the ^{7}Li resonance in the in–situ NMR spectra of the Li–Ge system by a structural transformation from Li_7Ge_3 to Li_7Ge_2 predicted by AIRSS and the species swapping method[19] .

New stable Li_2Sn–*Cmcm*, Li_8Sn_3–$R\bar{3}m$ and Li_7Sn_2–$P\bar{1}$ phases were predicted by the combined AIRSS + species swapping approach. Li_8Sn_3 was not considered in the analysis of the phase diagram of the Li–Sn system presented by Sanger *et al.*[2] However, a previous study performed by Gasior *et al.*[42] suggested its existence. To the best of our knowledge, this is the first time its structure has been presented. Li_2Sn–*Cmcm* has been obtained by AIRSS and is 1 meV/atom above the convex hull. The distance is well within DFT accuracy and comparable with known Li–Sn phases such as Li_5Sn_2 and Li_7Sn_3. We have analysed the mechanical stability of the Li_2Sn–*Cmcm* phase and found no negative phonon frequencies, suggesting that the structure should be mechanically stable at 0 K. An ill–defined form of Li_7Sn_2 has been observed at the end of lithiation of TiSbSn anodes.[14,15] We hypothesise that the less ordered Li_7Sn_2–$P\bar{1}$ phase revealed by AIRSS can form under certain electrochemical conditions, explaining the misfit between *Operando* Mossbauer spectra and the fit using the Li_7Sn_2–*Cmmm* phase.[14]

The Li_1Sn_1 phase obtained by AIRSS presents a layered arrangement similar to those observed in the Li–Si and Li–Ge systems[18] which were predicted to be stable at high–pressures. Interestingly, different phases with very similar ionic arrangement were obtained within a formation energy of 8 meV/atom. Within this range are also found the known the $P2/m$ and $I4_1/amd$ Li_1Sn_1 structures. Li_1Sn_1–*Pmm*2 is found 7 meV/atom above the Li_1Sn_1–$P2/m$ ground state and 1 meV below Li_1Sn_1–$I4_1/amd$.

From the stable structures found on the convex hull we have calculated the theoretical voltage

curve. Our theoretical voltage curve was obtained mainly from experimentally known structures and shows an excellent agreement with the coulometric titration experiment reported in Ref. 4 at 400°C for $x > 1$. The discrepancy between the calculated and experimental (coulometric titration) voltage curves in $2 < x < 2.6$ arises from the fact that Li_7Sn_3 and Li_5Sn_2 were not included in the voltage curve calculation, since only stable structures were considered. Below $x = 1$, the high–temperature experimental voltage curve shows a sloped shape due to liquid state of Sn–rich phases at 400°C.[43] The room temperature coulometric titration experiment shows well defined plateaus also below $x = 1$. First, a voltage drop is observed at $x = 0.4$, which has been attributed to Li_2Sn_5 and is well described by our calculated voltage curve. However, a major discrepancy is observed at $x \approx 0.66$, where a sharp voltage drop in the experimental voltage curve is not reproduced by our theoretical calculation. AIRSS predicts a Li_2Sn_3–$P\bar{1}$ phase 6 meV/atom from the convex hull. The proximity of the structure to the convex hull suggests that this potential candidate could form under specific electrochemical conditions. The formation of a Li_2Sn_3 phase has been previously discussed,[44] but its crystalline structure has never been reported. For $x > 2.6$ in Li_xSn, our calculated voltage curve describes remarkably well the high–temperature experiment reported by Wang *et al.*[4] but not the low–temperature experiment which shows plateaus positioned at the same stoichiometries but at higher voltages. The differences between the experiments at different temperatures beyond $x = 2.6$ (hundreds of meVs) can not be justified by entropic effects which were measured[45] to be of the order of tens of meVs. Based on these findings we hypothesise that the 25 °C experiment is diffusion limited; however, further work is needed to fully understand whether the difference in the voltage is due to diffusion limitations or kinetically driven. Both attempts by Courtney and Tran fail to describe the experimental voltage curves beyond $x = 2.5$. Our convex hull shows that the $x \leq 2.5$ and $x \geq 2.5$ regimes are separated by the formation of Sn–Sn dumbbells at $x = 2.5$ which can facilitate the single phase reaction observed at $x \geq 2.5$. We believe that in the galvanostatic test the system evolves via two-phase reactions up to the dumbbell region and from there it goes to a single-phase/amorphous regime. This has been seen in other systems such as Li–Ge, where dumbbells were predicted both in the metastable and stable regions over a range

of voltages. These were subsequently shown to interpret the NMR data (see Ref. 19 for details).

Our Li–Sb phase diagram is less rich with only three metastable phases appearing between $0 < x < 3$ in Li_3Sb within 30 meV/atom from the convex hull . Experimental studies observe only two stoichoimetries formed electrochemically, which correspond to the known Li_2Sb and both hexagonal and cubic Li_3Sb. The Li–Sb system exhibits a preference to form a layered phase with $P4/mmm$ symmetry at Li_1Sb_1, as observed in other systems such as Li–Si, Li–Ge and Li–Sn. Our search shows a variety of structures at $x > 3$ in Li_xSb close to the convex hull tie–line, some of them within the accuracy of the DFT functional and therefore indistinguishable from stable. AIRSS searches at almost all stoichiometries we tried in this regime find structures very close to the convex hull which suggests low formation energies of Sb interstitials in rich–lithium environments. Furthermore, these phases were found after only a few attempts hinting that these structures might be easy to form. We have further investigated the possible effect of formation of high–lithium content phases on the system electrochemistry by calculating the average voltages of the the lowest energy metastable structures, Li_4Sb, Li_5Sb and Li_6Sb, both in the absence and presence of Li_3Sb. Our results show that voltages drop to values close to zero when these phases are included. In Ref. 11 a comparison between cycle performances for different Sb composites using two voltage windows, 0.8–2.0 V and 0.0–2.0 V, is presented (see Figure 5 therein). The Sb/C composite operating within 0.8–2.0 V was shown to perform significantly better compared to the same anode cycled within the voltage range between 0.0 and 2.0 V. The difference in the performance was mainly attributed to degradation caused due to large volume changes originating in the formation of Li_3Sb when using the voltage window of 0.0–2.0 V. However, large volume changes also occur when lithiating to Li_2Sb ($\Delta V/V = 93\%$, comparable to volume expansion in Al anodes[46]), without much performance degradation, hence we suggest that the formation of highly–lithiated phases also play a part in efficiency degradation due to the proximity their voltage to Li which can cause lithium–plating.

Ex situ NMR measurements reported in Ref. 15 reveal two positive shifts at 3.8 and 7 ppm which have been assigned to Li_3Sb–related phases. The 7 ppm resonance was suggested to corre-

spond to a Li defect site in Li_3Sb (see the Supporting Information therein for details). In addition, a series of negative resonances were reported and ascribed to changes in the electronic structure.[15] Not only negative resonances make the full interpretation of the NMR pattern challenging, but also possible contributions from hexagonal–Li_3Sb (observed in minor fractions in Ref. 9) and off stoichiometry $Li_{3-\delta}Sb$ (formation of vacancies in the Li tetrahedral sites as suggested in Ref. 15). The present implementation of the GIPAW algorithm[28] enables us to access numerically the chemical shielding of phases with a finite band gap in the electronic density of states. We have calculated the NMR chemical shifts of the Li_3Sb $Fm\bar{3}m$ and $P6_3/mmc$ phases, which are of particular interest since it has been suggested that both form during the electrochemical process.[9] Our GIPAW calculations for the cubic–Li_3Sb phase reveal two resonances at 3.1 (the octahedral site) and 9.1 ppm (from two tetrahedral sites). For the hexagonal–Li_3Sb phase, two resonances are found at 9.7 and 6.6 ppm. An illustration with the resulting chemical shift is presented in Figure 10. These

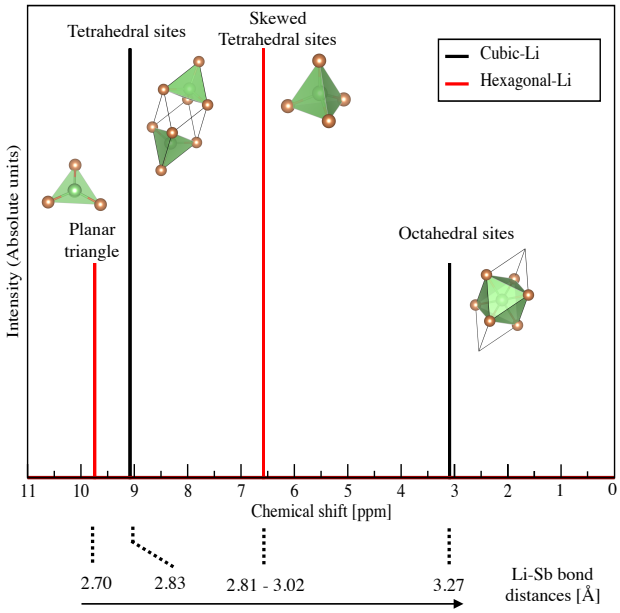

Figure 10: Calculated ^{7}Li NMR chemical shifts of the Li_3Sb $Fm\bar{3}m$ and $P6_3/mmc$ phases showing two resonances at 3.1 (the octahedral site) and 9.1 ppm (from two tetrahedral sites) arising from the cubic–Li_3Sb phase and two resonances at 9.7 and 6.6 ppm from the hexagonal–Li_3Sb phase. Li–Sb distances corresponding to each site are also shown. The ^{7}Li shifts were referenced using a secondary reference, Li_2CO_3, at +1.1 ppm versus the 1.0 M LiCl (aq) primary reference at 0.0 ppm.

were also calculated at two different pressures, both 2 and -2 GPa, where a maximum difference of 1 ppm was obtained suggesting that the results are robust with respect to volume changes associated with our choice of exchange–correlation functional. The calculated chemical shifts are close to the positive resonances observed in Ref. 15. Our results provide for first time robust first principles chemical shifts for both phases which can be used as a diagnostic tool to evaluate relative contributions from octahedral and tetrahedral sites in cubic–Li_3Sb and peak positions for both the hexagonal and cubic phases. In addition, the calculations revealed a trend in the Li–Sb bond distances which is found to increase as the chemical shift decreases.

Conclusions

Despite several studies in the Li–Sn / Li–Sb systems, lithiation mechanisms are still far from being well–understood. We have performed a structure prediction study to give a better understanding of possible structural arrangements in these systems. The unique capability of AIRSS has provided access to metastable structures and enabled us to identify possible general structural evolutions of Sn and Sb under lithiation, from layers, through zig-zag-chains, then dumbbells to isolated atoms. Since our extensive searches find no structures near the hull which do not obey these trends, we believe these motifs to be dominant during cycling. This insight could not have been gained from structure databases since the metastable structures are also required to uncover the trends in the lithiation process, even if they play a minimal role in the voltage curves. We have discovered new phases including Li_2Sn–*Cmcm*, Li_8Sn_3–$R\bar{3}m$ and Li_7Sn_2–$P\bar{1}$, which aid in the interpretation of subsequent experimental observations. The calculated voltage curve of the Li–Sn system was obtained mainly from experimentally known structures and shows good agreement to the experimentally observed voltage curve. Previous voltage curves presented were compared against standard galvanostatic and this is the first time, to the best of our knowledge, that a comparison between the DFT voltage curve and coulometric titration experiments has been made. We believe that the predictive nature of this work will stimulate an experimental revision of the system and

the new structures and structural trends discovered provide important insights about the system. The new candidate phases discovered in this work will play a significant role in subsequent high quality experimental investigations, in particular of multi-species electrodes such as LiSnSb and LiSnSbTi, where the need for a detailed (beyond the voltage profile) understanding of structures becomes more acute. By performing first principles NMR calculations, we have elucidated the origin of the stoichiometric Li_3Sb references of both the hexagonal and cubic phases. We have described the expected relative intensities and local oder corresponding to each site and showed a trend in the NMR chemical shift as Li–Sb bond distances change. These results were compared to findings of Johnston *et al.*, *Chemistry of Materials* (2016) *28*, 4032 and proposed as a tool for better understanding of experimental studies.

In summary, our study helps to understand previous experimental findings and provide a detailed description of possible structural arrangements that can aid the interpretation of future findings and guide experimental studies.

Acknowledgement

M.M. and A.J.M. acknowledge the support from the Winton Programme for the Physics of Sustainability.

Supporting Information Available

Additional research data supporting this publication, including CIF files of the structures obtained by AIRSS and species-swapping methods, are available as supplementary files at the journal's website. This material is available free of charge via the Internet at `http://pubs.acs.org/`.

References

(1) Obrovac, M.; Chevrier, V. Alloy Negative Electrodes for Li-ion Batteries. *Chemical reviews* **2014**, *114*, 11444–11502.

(2) Sangster, J.; Bale, C. W. The Li-Sn (Lithium-Tin) system. *Journal of Phase Equilibria* **1998**, *19*, 70–75.

(3) Goward, G.; Taylor, N.; Souza, D.; Nazar, L. The True Crystal structure of Li 17 M 4 (M= Ge, Sn, Pb)–Revised From Li 22 M 5. *Journal of alloys and compounds* **2001**, *329*, 82–91.

(4) Wang, J.; Raistrick, I.; Huggins, R. Behavior of Some Binary Lithium Alloys as Negative Electrodes in Organic Solvent-Based Electrolytes. *Journal of The Electrochemical Society* **1986**, *133*, 457–460.

(5) Courtney, I.; Tse, J.; Mao, O.; Hafner, J.; Dahn, J. Ab Initio Calculation of the Lithium-tin Voltage Profile. *Physical Review B* **1998**, *58*, 15583.

(6) Tran, T. T.; Obrovac, M. Alloy negative electrodes for high energy density metal-ion cells. *Journal of The Electrochemical Society* **2011**, *158*, A1411–A1416.

(7) Jain, A.; Ong, S. P.; Hautier, G.; Chen, W.; Richards, W. D.; Dacek, S.; Cholia, S.; Gunter, D.; Skinner, D.; Ceder, G.; Persson, K. a. The Materials Project: A materials genome approach to accelerating materials innovation. *APL Materials* **2013**, *1*, 011002.

(8) Baker, H. *ASM Handbook: Vol. 3 [electronic resource] Alloy Phase Diagrams*, 10th ed.; A S M International: Materials Park, 1992.

(9) Baggetto, L.; Ganesh, P.; Sun, C.-N.; Meisner, R. A.; Zawodzinski, T. A.; Veith, G. M. Intrinsic thermodynamic and kinetic properties of Sb electrodes for Li-ion and Na-ion batteries: experiment and theory. *J. Mater. Chem. A* **2013**, *1*, 7985–7994.

(10) Hewitt, K.; Beaulieu, L.; Dahn, J. Electrochemistry of InSb as a Li Insertion Host: Problems and Prospects. *Journal of The Electrochemical Society* **2001**, *148*, A402–A410.

(11) Park, C.-M.; Yoon, S.; Lee, S.-I.; Kim, J.-H.; Jung, J.-H.; Sohn, H.-J. High-rate capability and enhanced cyclability of antimony-based composites for lithium rechargeable batteries. *Journal of The Electrochemical Society* **2007**, *154*, A917–A920.

(12) Chang, D.; Huo, H.; Johnston, K. E.; Ménétrier, M.; Monconduit, L.; Grey, C. P.; Van der Ven, A. Elucidating The Origins of Phase Transformation Hysteresis During Electrochemical Cycling of Li–Sb Electrodes. *Journal of Materials Chemistry A* **2015**, *3*, 18928–18943.

(13) Trifonova, A.; Wachtler, M.; Winter, M.; Besenhard, J. O. Sn-Sb and Sn-Bi alloys as anode materials for lithium-ion batteries. *Ionics* **2002**, *8*, 321–328.

(14) Sougrati, M. T.; Fullenwarth, J.; Debenedetti, A.; Fraisse, B.; Jumas, J.-C.; Monconduit, L. TiSnSb a new efficient negative electrode for Li-ion batteries: mechanism investigations by operando-XRD and Mössbauer techniques. *Journal of Materials Chemistry* **2011**, *21*, 10069–10076.

(15) Johnston, K. E.; Sougrati, M. T.; Stievano, L.; Darwiche, A.; Dupré, N.; Grey, C. P.; Monconduit, L. The effects of relaxation on conversion negative electrode materials for Li-ion batteries: a study of TiSnSb using 119Sn Mössbauer and 7Li MAS NMR spectroscopies. *Chemistry of Materials* **2016**,

(16) Pickard, C. J.; Needs, R. J. High-Pressure Phases of Silane. *Phys. Rev. Lett.* **2006**, *97*, 045504.

(17) Pickard, C. J.; Needs, R. J. *Ab Initio* Random Structure Searching. *J. Phys.: Condens. Matter* **2011**, *23*, 053201.

(18) Morris, A. J.; Grey, C. P.; Pickard, C. J. Thermodynamically Stable Lithium Silicides and Germanides From Density Functional Theory Calculations. *Phys. Rev. B* **2014**, *90*, 054111.

(19) Jung, H.; Allan, P. K.; Hu, Y.-Y.; Borkiewicz, O. J.; Wang, X.-L.; Han, W.-Q.; Du, L.-S.; Pickard, C. J.; Chupas, P. J.; Chapman, K. W.; Morris, A. J.; Grey, C. P. Elucidation of the Local and Long-Range Structural Changes that Occur in Germanium Anodes in Lithium-Ion Batteries. *Chem. Mater.* **2015**, *27*, 1031–1041.

(20) See, K. A.; Leskes, M.; Griffin, J. M.; Britto, S.; Matthews, P. D.; Emly, A.; Van der Ven, A.; Wright, D. S.; Morris, A. J.; Grey, C. P.; Seshadri, R. Ab Initio Structure Search and in Situ

7Li NMR Studies of Discharge Products in the Li-S Battery System. *J. Am. Chem. Soc.* **2014**, *136*, 16368–16377, PMID: 25384082.

(21) Mayo, M.; Griffith, K. J.; Pickard, C. J.; Morris, A. J. Ab Initio Study of Phosphorus Anodes for Lithium-and Sodium-Ion Batteries. *Chemistry of Materials* **2016**, *28*, 2011–2021.

(22) George, C.; Morris, A. J.; Modarres, M. H.; De Volder, M. Structural Evolution of Electrochemically Lithiated MoS2 Nanosheets and the Role of Carbon Additive in Li-Ion Batteries. *Chemistry of Materials* **2016**, *28*, 7304–7310.

(23) Morris, A. J.; Needs, R. J.; Salager, E.; Grey, C. P.; Pickard, C. J. Lithiation of Silicon via Lithium Zintl-Defect Complexes From First Principles. *Phys. Rev. B* **2013**, *87*, 174108.

(24) Clark, S. J.; Segall, M. D.; Pickard, C. J.; Hasnip, P. J.; Probert, M. J.; Refson, K.; Payne, M. First Principles Methods Using CASTEP. *Z. Kristall.* **2005**, *220*, 567–570.

(25) Perdew, J. P.; Burke, K.; Ernzerhof, M. Generalized Gradient Approximation Made Simple. *Phys. Rev. Lett.* **1996**, *77*, 3865–3868.

(26) Monkhorst, H. J.; Pack, J. D. Special Points for Brillouin-Zone Integrations. *Phys. Rev. B* **1976**, *13*, 5188–5192.

(27) Aydinol, M. K.; Kohan, A. F.; Ceder, G.; Cho, K.; Joannopoulos, J. *Ab Initio* Study of Lithium Intercalation in Metal Oxides and Metal Dichalcogenides. *Phys. Rev. B* **1997**, *56*, 1354–1365.

(28) Pickard, C.; Mauri, F. All-Electron Magnetic Response With Pseudopotentials: NMR Chemical Shifts. *Phys. Rev. B* **2001**, *63*, 245101.

(29) Refson, K.; Tulip, P. R.; Clark, S. J. Variational Density-Functional Perturbation Theory for Dielectrics and Lattice Dynamics. *Phys. Rev. B* **2006**, *73*, 155114.

(30) Hansen, D.; Chang, L. Crystal structure of Li2Sn5. *Acta Crystallographica Section B: Structural Crystallography and Crystal Chemistry* **1969**, *25*, 2392–2395.

(31) Müller, W.; Schäfer, H. The Crystal Structure of the LiSn Compound. *Z. Naturforsch. B* **1973**, *28*, 246–248.

(32) Müller, W. Darstellung und Struktur der Phase Li7Sn3/Preparation und Crystal Structure of Li7Sn3. *Zeitschrift für Naturforschung B* **1974**, *29*, 304–311.

(33) Frank, U.; Müller, W.; Schäfer, H. Die Struktur der Phase Li5Sn2/The Crystal Structure of Li5Sn2. *Zeitschrift für Naturforschung B* **1975**, *30*, 1–5.

(34) Frank, U.; Müller, W. Darstellung und Struktur der Phase Li13Sn5 und die strukturelle Verwandtschaft der Phasen in den Systemen Li-Sn und Li-Pb/The Preparation and Crystal Structure of Li13Sn5 and the Structural Relations Between the Phases of the Systems Li-Sn and Li-Pb. *Zeitschrift für Naturforschung B* **1975**, *30*, 316–322.

(35) Zalkin, A.; Ramsey, W.; Templeton, D. Intermetallic Compounds between Lithium and Lead. II. The Crystal Structure of Li8Pb3. *The Journal of Physical Chemistry* **1956**, *60*, 1275–1277.

(36) Frank, U.; Müller, W.; Schäfer, H. Die Kristallstruktur der Phase Li7Sn2/The Crystal Structure of Li7Sn2. *Zeitschrift für Naturforschung B* **1975**, *30*, 6–9.

(37) Zintl, E.; Harder, A. Zur Stoechiometrie binaerer Natriumverbindungen. (21. Mitteilung ueber Metalle und Legierungen). *Zeitschrift fuer Physikalische Chemie, Abteilung B: Chemie der Elementarprozesse, Aufbau der Materie* **1936**, *34*, 238–254.

(38) Zalkin, A.; Ramsey, W. Intermetallic compounds between lithium and lead. IV. The crystal structure of Li22 Pb5. *Journal of Physical Chemistry* **1958**, *62*, 689–693.

(39) Blase, W.; Cordier, G. Crystal structure of β-Lithium stannide, β-LiSn. *Zeitschrift für Kristallographie-Crystalline Materials* **1990**, *193*, 317–318.

(40) Müller, W. Notizen: Darstellung und Struktur der Phase Li2Sb/Preparation and Crystal Structure of Li2Sb. *Zeitschrift für Naturforschung B* **1977**, *32*, 357–359.

(41) Brauer, G.; Zintl, E. Konstitution von Phosphiden, Arseniden, Antimoniden und Wismutiden des Lithiums, Natriums und Kaliums. (23: Mitteilung ueber Metalle und Legierungen.). *Zeitschrift fuer Physikalische Chemie, Abteilung B: Chemie der Elementarprozesse, Aufbau der Materie* **1937**, *37*, 323–352.

(42) Gasior, W.; Moser, Z.; Zakulski, W. Ninth International Conference on Liquid and Amorphous Metals Thermodynamic studies and the phase diagram of the Li-Sn system. *Journal of Non-Crystalline Solids* **1996**, *205*, 379 – 382.

(43) Huggins, R. A. Lithium alloy negative electrodes. *Journal of Power Sources* **1999**, *81*, 13–19.

(44) Barsukov, I. V.; Johnson, C. S.; Doninger, J. E.; Barsukov, V. Z. *New Carbon Based Materials for Electrochemical Energy Storage Systems: Batteries, Supercapacitors and Fuel Cells*; Springer Science & Business Media, 2006; Vol. 229.

(45) Wen, C. J.; Huggins, R. A. Thermodynamic study of the lithium-tin system. *Journal of The Electrochemical Society* **1981**, *128*, 1181–1187.

(46) Liu, Y.; Hudak, N. S.; Huber, D. L.; Limmer, S. J.; Sullivan, J. P.; Huang, J. Y. In situ transmission electron microscopy observation of pulverization of aluminum nanowires and evolution of the thin surface Al2O3 layers during lithiation–delithiation cycles. *Nano letters* **2011**, *11*, 4188–4194.

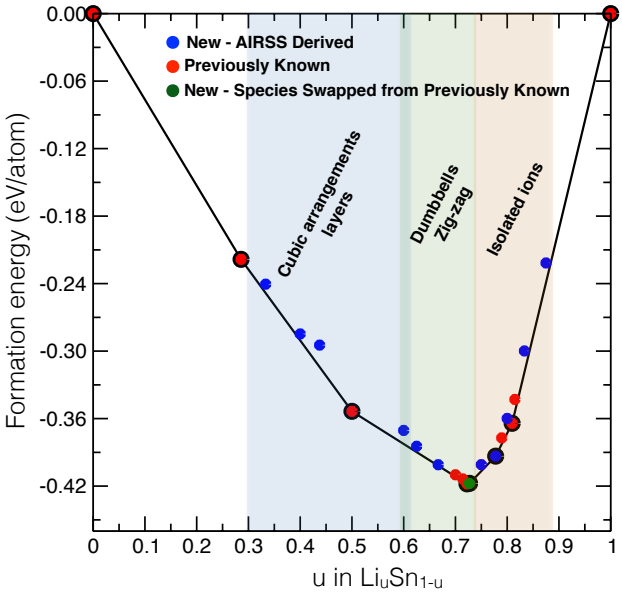

Figure 11: ToC